ARTICLE OPEN ACCESS

Hot Corrosion Type X: Behavior of Mo-Si-B at Different Temperatures

Lukas Korell[1] | Katharina Beck[1] | Ceyhun Oskay[1] | Daniel Schliephake[2] | Martin Heilmaier[2] | Mathias C. Galetz[1]

[1]High Temperature Materials, DECHEMA-Research Institute, Bad Homburg, Hessen, Germany | [2]Institute for Applied Materials, Karlsruhe Institute of Technology, Karlsruhe, Baden-Würtemberg, Germany

Correspondence: Lukas Korell (lukas.korell@dechema.de)

Received: 16 January 2026 | **Revised:** 19 August 2026 | **Accepted:** 31 August 2026

Funding: Deutsche Forschungsgemeinschaft, Grant/Award Number: 413956820

Keywords: eutectics | hot corrosion | Mo-Si-B | molten salts | Na_2SO_4 | pesting

ABSTRACT

To improve gas turbine efficiencies, temperatures must increase, necessitating new materials that can operate beyond the temperature limits of Ni-based alloys. Due to their high melting points and creep strength, novel material candidates contain refractory elements. Molybdenum (Mo)-based Mo-Si-B alloys have been investigated for more than 20 years. Surprisingly, their hot corrosion behavior was not investigated in detail. For Ni-based alloys, two mechanisms are established: Corrosion due to melting of Na_2SO_4 (Type I, ~900°C) or due to the formation of lower-melting eutectics (Type II, ~700°C). In this work, the temperature-dependent mechanism for Mo-Si-B is investigated, by studying the hot corrosion resistance of Mo-Si-B at 500°C–900°C. Post-testing analysis via XRD, SEM, Raman and EPMA is used to reveal the degradation mechanisms. Na_2MoO_4, which forms under Na_2SO_4 deposits, is responsible for dissolving the surrounding material due to its lower melting point in respect to Na_2SO_4. This alters the mechanism to a super-acidic Na-Mo-based attack (Type X hot corrosion). Finally, these results can trigger mitigation strategies, such as protective coatings for Mo-based systems.

1 | Introduction

Ni-based alloys are the gold standard for high-temperature applications such as turbine blades [1, 2]. For even higher operating temperatures than those currently achievable, refractory element alloys are promising candidates. Their high melting points can potentially increase the maximum metal temperatures from 1150°C to 1400°C or more. By increasing the operating temperature and reducing cooling losses, efficiency can be enhanced [2, 3]. Because of their high creep resistance and microstructural stability at elevated temperatures, Mo-Si-B alloys have attracted attention for more than three decades, since the first introduction of the system by Berczaik and Akinc [4, 5]. While significant improvements have been achieved in their oxidation behavior [6, 7], their resistance to Na_2SO_4 has received little attention. One of the most corrosive environments in the turbine is triggered by salts that deposit on the turbine blades [8–11]. Na_2SO_4 is considered the most critical component in what became famous as "hot corrosion" [9, 12–15]. NaCl resulting from sea salt reacts with sulfur-containing impurities in fuel or air to form Na_2SO_4, as displayed in Equation (1) [9, 15].

$$2NaCl(g) + SO_3(g) + 2\,O_2(g) \rightleftharpoons Na_2SO_4(l) + Cl_2(g) \quad (1)$$

In hot corrosion, two separate mechanisms are established for Ni-based alloys, based on the Na_2SO_4 melting point of 884°C [16]. Melting of the salt results in a liquid phase, causing a uniform corrosion attack with a high corrosion rate [13, 17]: hot

corrosion Type I. Hot corrosion Type II is based on the formation of low-melting mixtures between the salt and corrosion products, e.g. $CoSO_4$–Na_2SO_4 ($T_m = 540°C$) or $NiSO_4$–Na_2SO_4 ($T_m = 670°C$) [8, 9, 18, 19]. In contrast to the uniform attack from hot corrosion Type I, Type II is characterized by localized pit formation [8, 20]. Recently, newer Mo-Si-Ti alloys were developed that exhibit highly improved oxidation behavior in the hot corrosion temperature range, making it interesting to characterize and understand the hot corrosion behavior of Mo-based alloys in detail [21–24]. Ni-based alloys show an enhanced corrosion rate in the presence of Na_2SO_4 deposits when their composition contains Mo [14]. In this case, Na_2SO_4 is converted to Na_2MoO_4 with a melting point of 687°C, which can introduce basic fluxing and rapid corrosion of Ni-alloys [14, 25, 26]. A recent study showed that the hot corrosion behavior of Mo-20Si-52.8Ti and Mo-21Si-34Ti differs significantly from that of Ni-based alloys [27, 28].

Another significant limitation of Mo-based alloys is their low inherent oxidation resistance, as they are prone to catastrophic oxidation behavior known as "Pesting." This is characterized by the dominant formation of volatile MoO_3. This results in strong oxidation from around 700°C whereas a protective SiO_2 scale is produced at higher temperatures, such as 1300°C [6, 21, 29–31].

Exposure of Mo-9Si-8B (at.%) in SO_2-containing atmosphere with a Na_2SO_4 deposit at 700°C and 900°C resulted in a discontinuous SiO_2 layer that could not protect against pesting [29].

To identify which degradation mechanisms participate at different temperatures in the hot corrosion of Mo-based alloys and determine the temperature regimes of the different corrosion mechanisms, in this work corrosion tests were carried out at 500°C, 600°C and 800°C on Mo-9Si-8B (at.%) in an atmosphere consisting of synthetic air and 0.1% SO_2 with a deposit of 2.5 mg/cm^2 Na_2SO_4. Cross sections of the corroded samples were analyzed with XRD, SEM, EPMA and Raman spectroscopy to discuss the results. The tests were conducted in a manner consistent with those at 700°C and 900°C [29], and the combined results were utilized to obtain a comprehensive understanding of the hot corrosion behavior of Mo-8Si-9B (at%).

2 | Experimental

2.1 | Alloying

The Mo-9Si-8B (at.%) alloy was prepared by field-assisted sintering (FAST) from the elemental powders Mo (99.95%, HC Starck), Si (99.99%, Alfa Aesar), and B (98%, MaTeck), at 1600°C and 50 MPa hold for 15 min. The powders were mechanically alloyed in a planetary ball mill (Retsch PM 400) using WC balls, a powder-to-ball ratio of 1:12, with a speed of 200 rpm.

After compacting under vacuum at 5 hPa, the resulting buttons, which had a residual porosity of less than 2% [32], were subjected to a homogenization treatment at 1600°C for 100 h. Arc-wire cutting was used to cut specimens out of each alloy. Specimens 12 to 14 mm in diameter and 10 mm in height were cut from the Mo-Si-B buttons and finalized to 10 mm × 10 mm × 3 mm sample dimensions. After cutting, the samples were ground with P500 silicon carbide paper to remove Cu contamination, which have been introduced by wire erosion. The produced samples were cleaned with an ultrasonic bath in acetone.

2.2 | Hot Corrosion

For the hot corrosion experiments, 2.5 mg/cm^2 Na_2SO_4, which is a high amount with respect to the amount that can be encountered in normal operating conditions, was deposited by evaporating an aqueous solution onto preheated samples independently of the exposure time. The samples were placed in individual Al_2O_3 crucibles and put in a quartz tube furnace (Carbolite VST 12/900). After a drying step at 150°C under synthetic air for 12 h, the samples were exposed to dry synthetic air (99.99%, Air Liquide) mixed with 0.1 vol% SO_2 (99.98%, Air Liquide) with a flow rate of about 5 L/h. The furnace was heated to the designated temperature at a heating rate of 10°C/min. Experiments were conducted at 500°C, 600°C, and 800°C to compare the corrosion behavior at different temperatures. To investigate the development of hot corrosion over time, experiments were conducted for 24 and 100 h. A Fe_2O_3 catalyst was placed at the gas inlet of the furnace to enable the oxidation of SO_2 in the gas mixture to SO_3:

$$SO_2 + 1/2O_2 \rightleftharpoons SO_3 \quad (2)$$

After the experiment, the samples were cooled down to room temperature using natural cooling under pure synthetic air.

2.3 | Analytical Characterization

A Leica MZ16 stereomicroscope was used to take macroscopic images of the as-cast state and after hot corrosion experiments.

To perform X-ray diffraction (XRD) measurements, a Bruker D8 Advance A25 and Cu-Kα radiation were used. Cross sections of each sample were produced by mounting them in epoxy resin and cutting them in half. Cross sections were ground and polished using a series of silicon carbide papers to P2400 and diamond suspensions with 3 and 1 μm. The grinding and polishing were done using water-free petroleum as lubricant.

Subsequent analysis of the sample thickness was performed on microscopic images using IMS software and at least six measurements. The uncertainty represents the standard deviation of the individual measurements. After sputtering with graphite, a scanning electron microscope (SEM, Hitachi FlexSEM 1000II with an energy dispersive X-ray spectrometer (EDS)) was utilized to investigate the cross sections of the samples. The average of at least four separate measurements was calculated to determine the layer thicknesses and standard deviations. A JEOL JXA-8100 electron probe microanalyzer (EPMA), equipped with a wavelength dispersive detector (WDX), was used to produce each sample's concentration profiles and elemental mapping. Raman spectroscopy (Renishaw inVia Raman Microscope) was performed at 633 nm to further analyze the formed oxides.

3 | Results

Figure 1 shows the cross-section of Mo-9Si-8B (at.%) after the exposure at 500°C with Na_2SO_4 deposit including the elemental distributions.

After 24 h test at 500°C, a MoO_3 layer was found on the surface of the sample. On top of this layer, a $Na_2Mo_4O_{13}$ layer with incorporated particles of Na_2SO_4 and SiO_2 can be seen. All these phases were identified using XRD and Raman spectroscopy (see Figures A1 and A2 in the appendix). The thickness of the corrosion products exceeds 50 µm; Na is very evenly distributed throughout the outer layer, while sulfur can remain only locally.

After 100 h the overall oxide layer thickness stays in the same range as after 24 h. In this case, SiO_2 is consolidated in a denser layer on top of the MoO_3, with particles of Na_2SO_4 and Na_2MoO_4 locally enclosed (see Figure 1c,d).

Figure 2 displays the cross-section of Mo-9Si-8B (at.%) after the exposure at 600°C together with its elemental map.

After 24 h at 600°C, the same phases as at 500°C were detected using XRD and Raman spectroscopy, but the layer thickness had almost doubled. The MoO_3 layer and the $Na_2Mo_4O_{13}$, both detected by XRD and Raman (see Figures A1 and A2 in the appendix), thickened compared to the sample tested at 500°C. Some $Na_2Mo_4O_{13}$ particles are visible deeper inside the oxide layer than before, and SiO_2 particles are visible in the MoO_3 layer. At the same time, the silica appears more pronounced close to the surface.

After 100 h of hot corrosion at 600°C, SiO_2 is mostly found at the surface, but could not prevent the underlying material from oxidizing because no continuous layer formed. $Na_2Mo_4O_{13}$ is found deeper inside the oxide layer.

Figure 3 is adapted from [29] where the hot corrosion behavior of Mo-9Si-8B was tested at 700°C. It shows that at this temperature a continuous outer SiO_2 layer forms. After both exposure times MoO_3 is found underneath this layer in the form of large particles which are surrounded by cavities. Surprisingly, the overall corrosion layer was thicker after 24 h of exposure, whereas the SiO_2 layer thickened after 100 h. This can be explained by the densification and evaporation of MoO_3 which results in SiO_2 enrichment at the surface. Na is observed in the particles enclosed in the silica layer and inside the MoO_3 after both exposure times [29]. This effect cannot be observed at lower temperatures because the evaporation of MoO_3 is insufficient for a SiO_2 layer to form.

The cross-section of the Mo-9Si-8B (at.%) sample corroded at 800°C is presented in Figure 4. After just 24 h of hot corrosion at this temperature, most of the alloy was consumed. An oxide layer consisting of SiO_2 and MoO_3 is present on the sample

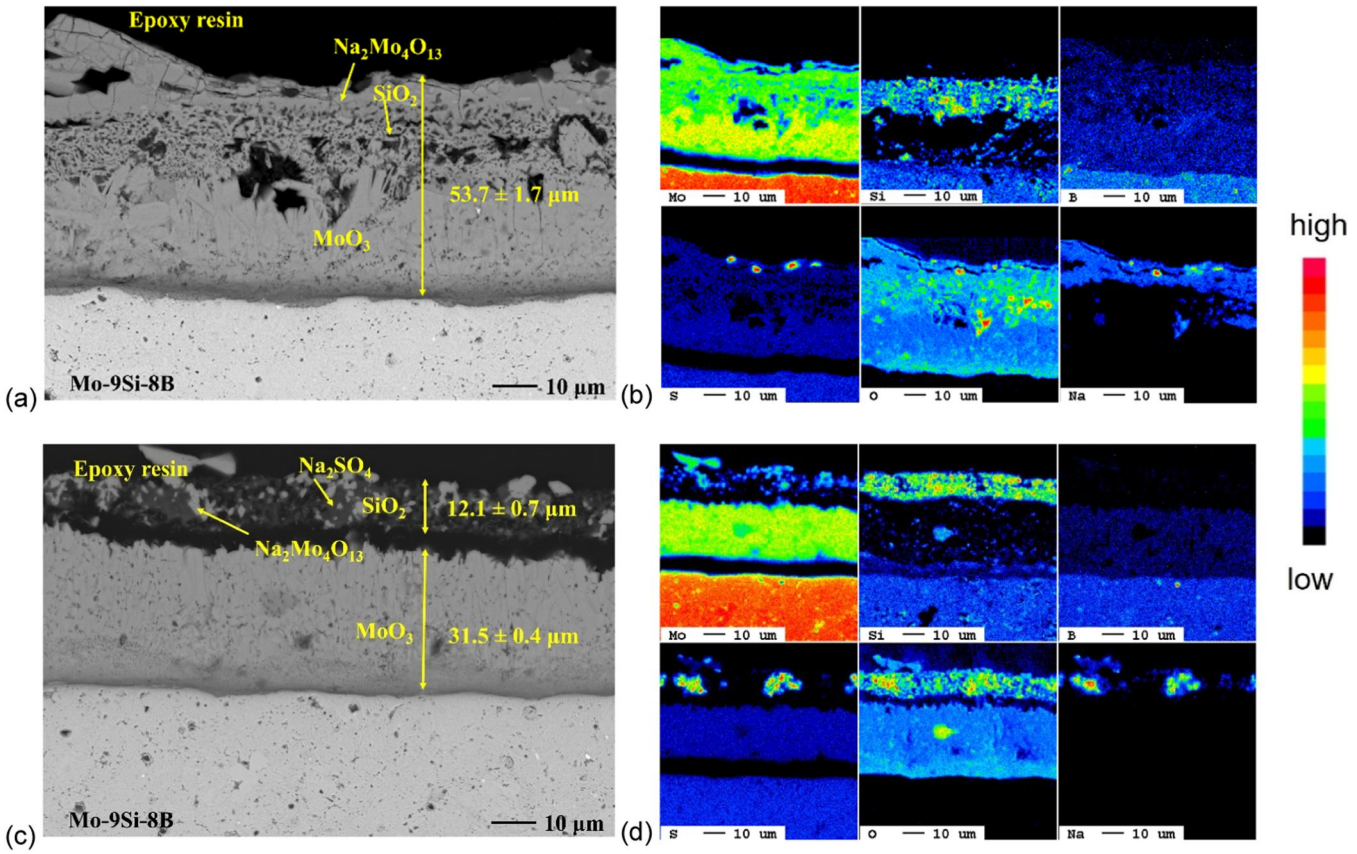

FIGURE 1 | (a, c) BSE images and (b, d) EPMA elemental maps of the cross section of Mo-9Si-8B (at.%) after 24 h (a, b) and after 100 h (c, d) of hot corrosion at 500°C 2.5 mg/cm^2 Na_2SO_4 deposit in synthetic air +0.1% SO_2. [Color figure can be viewed at wileyonlinelibrary.com]

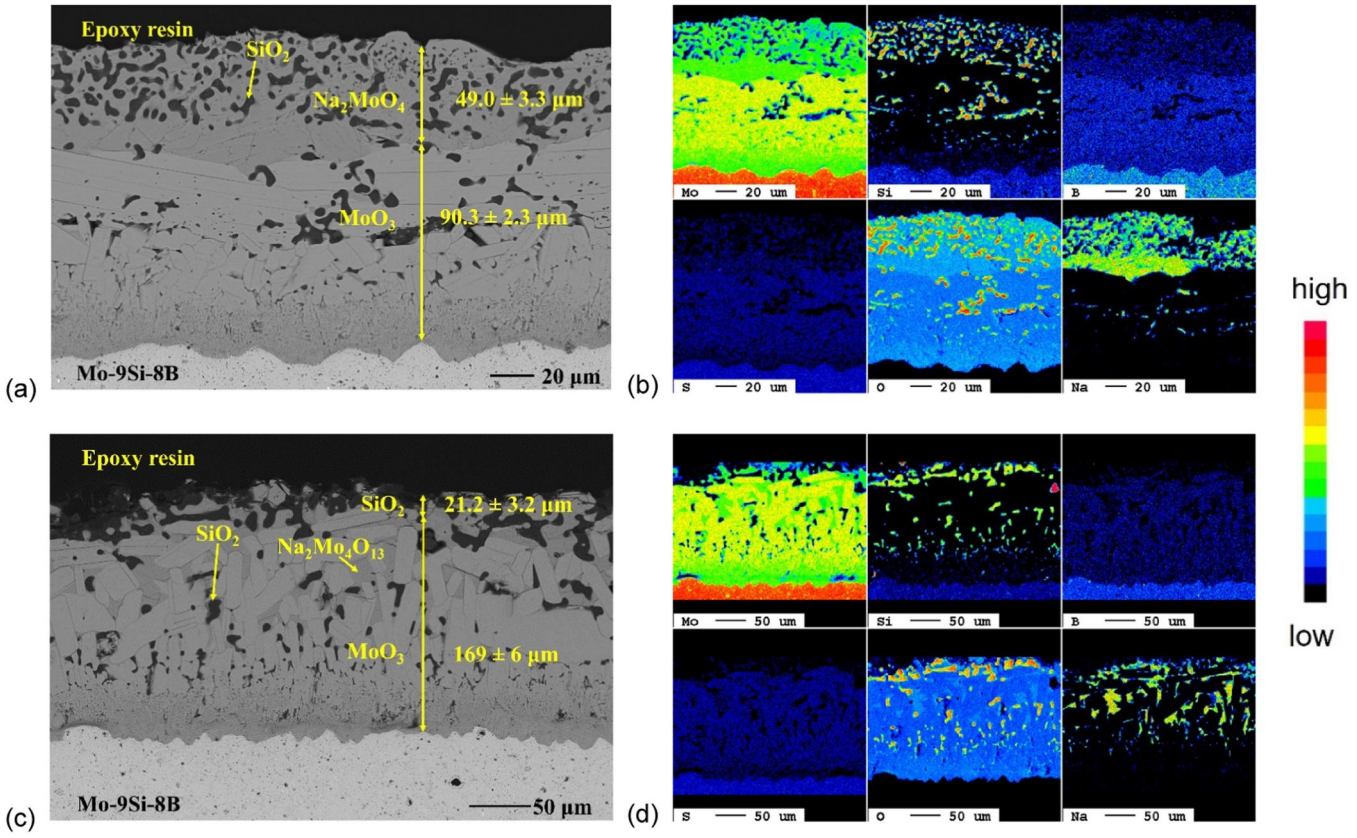

FIGURE 2 | (a, c) BSE images and (b, d) EPMA elemental map of the cross-section of Mo-9Si-8B (at.%) after 24 h (a, b) and after 100 h (c, d) of hot corrosion at 600°C with 2.5 mg/cm^2 Na_2SO_4 deposit in synthetic air +0.1% SO_2. [Color figure can be viewed at wileyonlinelibrary.com]

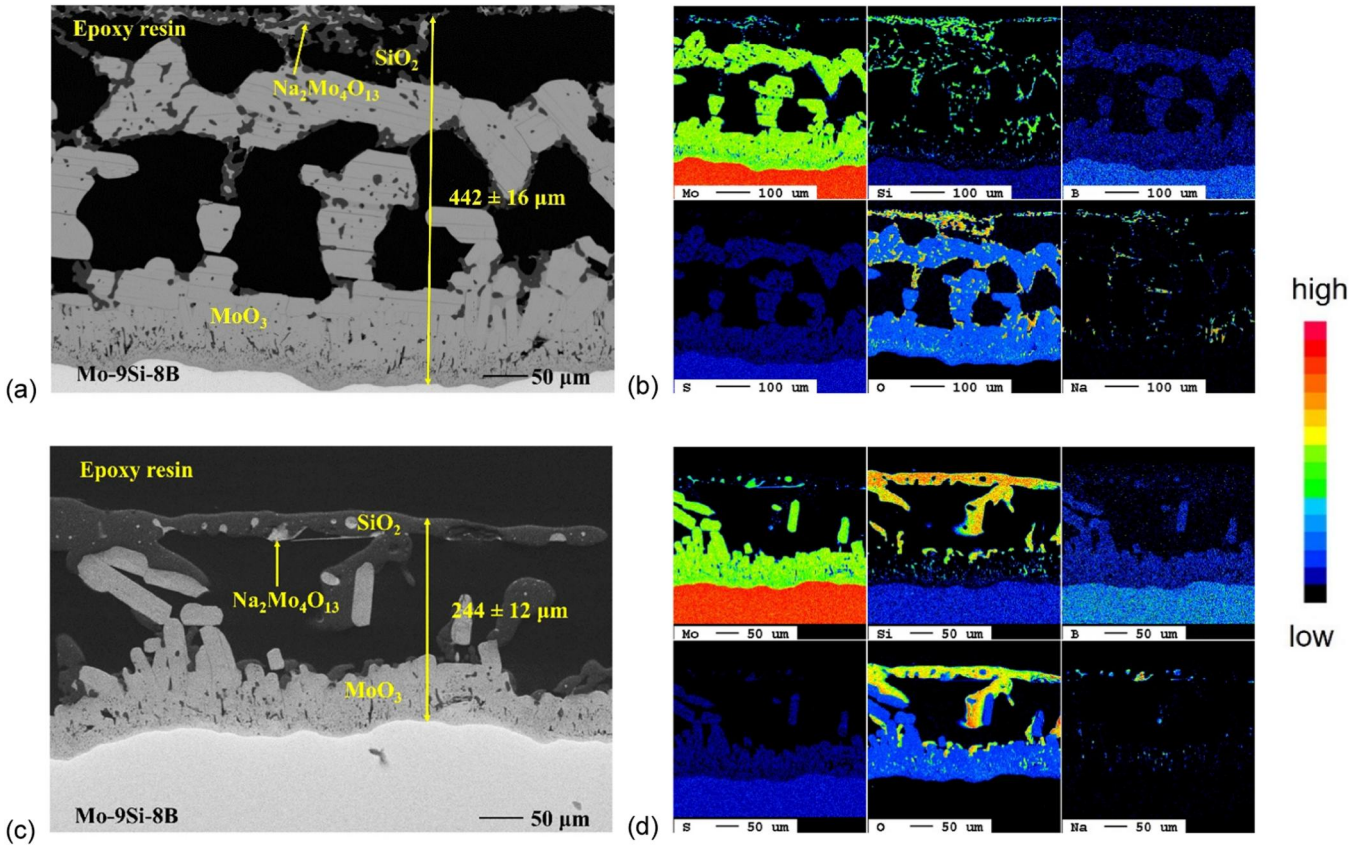

FIGURE 3 | (a, c) BSE images and (b, d) EPMA elemental map of the cross section of Mo-9Si-8B (at.%) after 24 h (a, b) and after 100 h (c, d) of hot corrosion at 700°C with 2.5 mg/cm^2 Na_2SO_4 deposit in synthetic air +0.1% SO_2. Adapted from [29]. [Color figure can be viewed at wileyonlinelibrary.com]

surface (see XRD Figure A1 in the appendix), enclosing large cavities. No Na could be found inside this structure. Spallation may have occurred during cooling because otherwise the MoO_3 found on the outer surface should have evaporated.

After 100 h the three-millimeter-thick metallic sample was fully consumed, and the resulting oxides were broken in pieces. The XRD signal reveals that the formed SiO_2 layer has a cristobalite structure (see Figure A1 in the appendix).

Only a small amount of Na was found on MoO_3 after exposure at 800°C.

The hot corrosion behavior of Mo-9Si-8B at 900°C was investigated in [29]. The corroded samples are displayed in Figure 5. A SiO_2 layer of around 150 µm formed after 24 h on a MoO_2 layer, which proves that this thick SiO_2 layer significantly reduced the oxygen partial pressure. After 100 h, almost the entire substrate was consumed by the corrosion process. The corrosion products mainly consisted of SiO_2 with MoO_3 precipitates. Following these exposures, almost no Na could be detected in the corrosion products [29].

4 | Discussion

Mo-Si-B alloy shows severe corrosion induced by the Na_2SO_4 deposit at temperatures as low as 500°C. In the first step, oxidation occurs which results in the oxides MoO_3, SiO_2 (and probably B_2O_3 — based on the EPMA qualitative signal for that element). Na_2MoO_4 is expected to form by a reaction of MoO_3 with the salt via Equation (3) [32].

$$Na_2SO_{4(s)} + MoO_{3(s)} \rightleftharpoons Na_2MoO_{4(s)} + SO_{3(g)} \quad (3)$$

Na_2MoO_4 and MoO_3 together both can form a low-melting phase with a melting point of 507°C [33–35]. This is significantly lower than those of Na_2MoO_4, melting at 687°C [15] and MoO_3, which has a melting point of 759°C [36]. Above these temperatures, liquid phases capable of dissolving the surrounding material are formed [37]. However, the severe corrosion as low as at 500°C can be explained by considering that the presence of the low-melting phase is proven, because it crystallizes during cooling to form $Na_2Mo_4O_{13}$ which was identified by XRD and Raman spectroscopy (see Figures A1 and A2 in the appendix) [35, 38]. The appearance of the liquid phase 7°C below its melting point can be explained by the presence of impurities.

This molten eutectic results in a significantly higher corrosion rate at much lower temperatures than that observed in Type II hot corrosion of Ni-based alloys. For the Mo-9Si-8B (at.%) alloy, molten salt enables a few more unexpected features, such as the formation of an outward-growing SiO_2 layer at the surface at 500°C, which is identified as quartz by XRD. During a solid-state reaction, silica typically oxidizes into an amorphous glass and not quartz at such temperatures. However, the layer formed

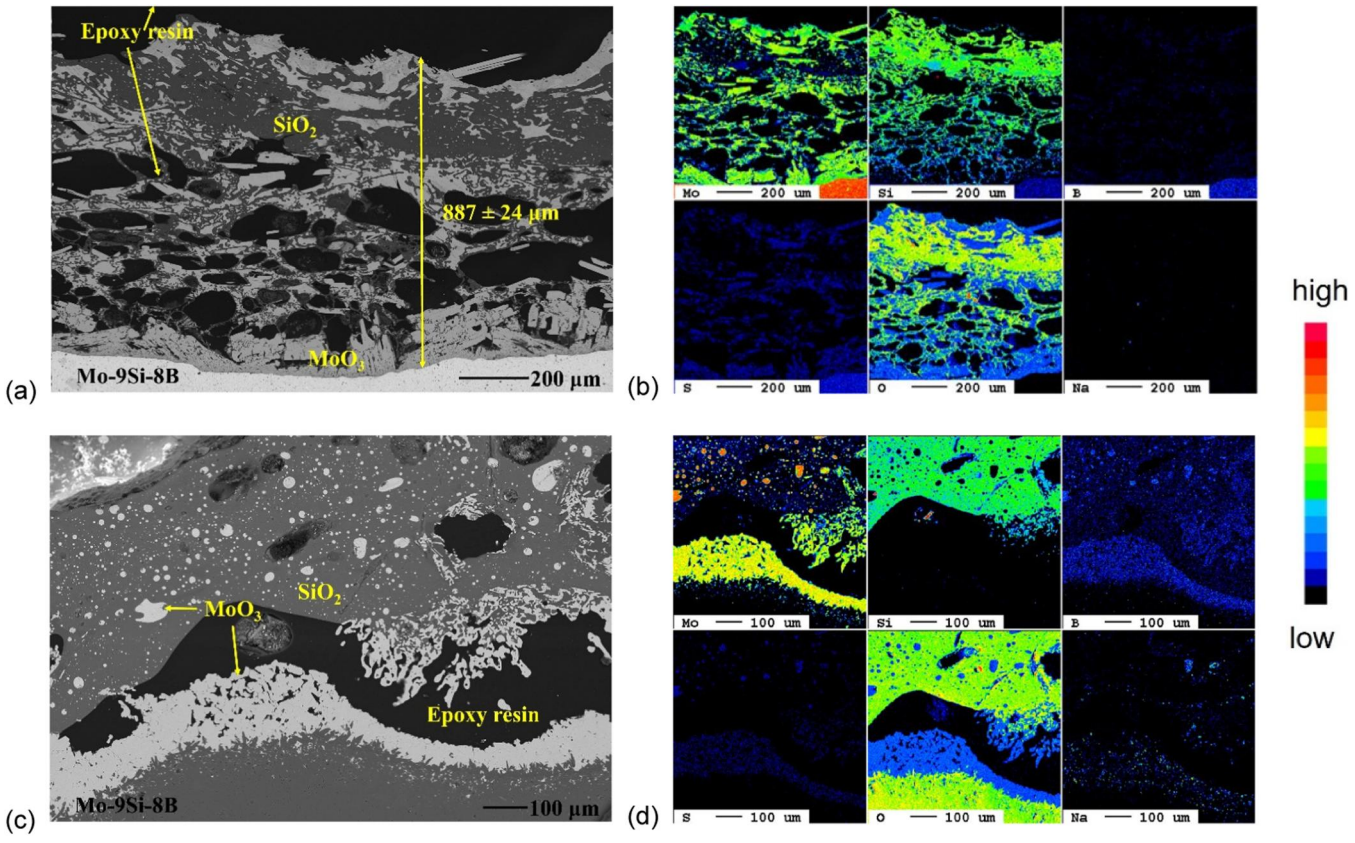

FIGURE 4 | (a, c) BSE images and (b, d) EPMA elemental map of the cross section of Mo-9Si-8B (at.%) after 24 h (a, b) and after 100 h (c, d) of hot corrosion at 800°C with 2.5 mg/cm^2 Na_2SO_4 deposit in synthetic air + 0.1% SO_2 – note the varying magnifications. [Color figure can be viewed at wileyonlinelibrary.com]

during the hot corrosion at 500°C and 600°C is not continuous and does not prevent the further degradation of the alloys. Even more interesting, after hot corrosion at 800°C and 900°C the SiO_2 layer formed on Mo-8Si-9B is identified as cristobalite by XRD (see Figure A1 in the appendix). Even though cristobalite is only stable at temperatures above 1470°C, its formation was observed before at 900°C when NaO_2 is present [11, 38]. NaO_2 results from the decomposition of Na_2SO_4 and acts as a network former, supporting the crystallization of SiO_2 [11, 39, 40]. Mo is known to undergo pesting, which describes the evaporation of MoO_3. Above 700°C, pesting is the dominant corrosion mechanism. The gaseous MoO_3 left behind visible cavities in the scale after exposure, when it vanished from the corroded structure. For Mo-9Si-8B (at.%) the SiO_2 could not protect the alloy at 800°C because of the pesting. At 900°C MoO_2 formed under the SiO_2 layer (see Figure 5) which proves that it provides some protection against rapid oxidation, but it could not stop the pesting, thus most of the Mo from the alloy evaporated during exposure [29].

The mechanisms of both pesting and formation of low melting phases were already observed to be detrimental in [25–30]. The results of [29] and this study were combined to plot a hot corrosion curve within the temperature range of 500°C–900°C. To estimate the corrosion rate, the change in thickness of the metallic samples was measured using the light microscopy images of the cross-sections after 24 and 100 h experiments and is presented in Table 1.

Based on the combined metal loss values after 24 and 100 h, the estimated corrosion curve presented in Figure 6 was drawn. It shows an increase in the corrosion rate from 500°C to 600°C. Within this temperature range, the eutectic MoO_3–Na_2MoO_4 melts and accelerates the corrosion rate (see Figures 1 and 2).

At 700°C, the corrosion in the first stage is higher than at lower temperatures because of the arising pesting and ongoing corrosion. After 24 h the formation of a nearly continuous SiO_2 layer was observed (see Figure 3) due to the volatilization of MoO_3 [29]. Once the layer is established, it significantly lowers the corrosion, resulting in a minimum of the corrosion rate thus diffusion through this layer must be the rate-limiting step. This layer formation has previously been observed in oxidation experiments [6, 25, 41]. At higher temperatures, the corrosion rate of Mo-9Si-8B (at.%) is rising because pesting becomes stronger with an increase in temperature. At 800°C and 900°C, the silica layer cannot stand against the high amount of pesting, and the alloy was fully consumed after 100 h (see Figures 4 and 5). In both cases, the metal loss is higher than 3 mm/100 h. From the results after 24 h of testing it can still be concluded that at 900°C the corrosion rate is lower. This can be explained by the softening of the SiO_2-rich layer which then can slow down the corrosion of the underlying material—even if only slightly [42], as bubbles of MoO_3 can move through the layer [31, 41].

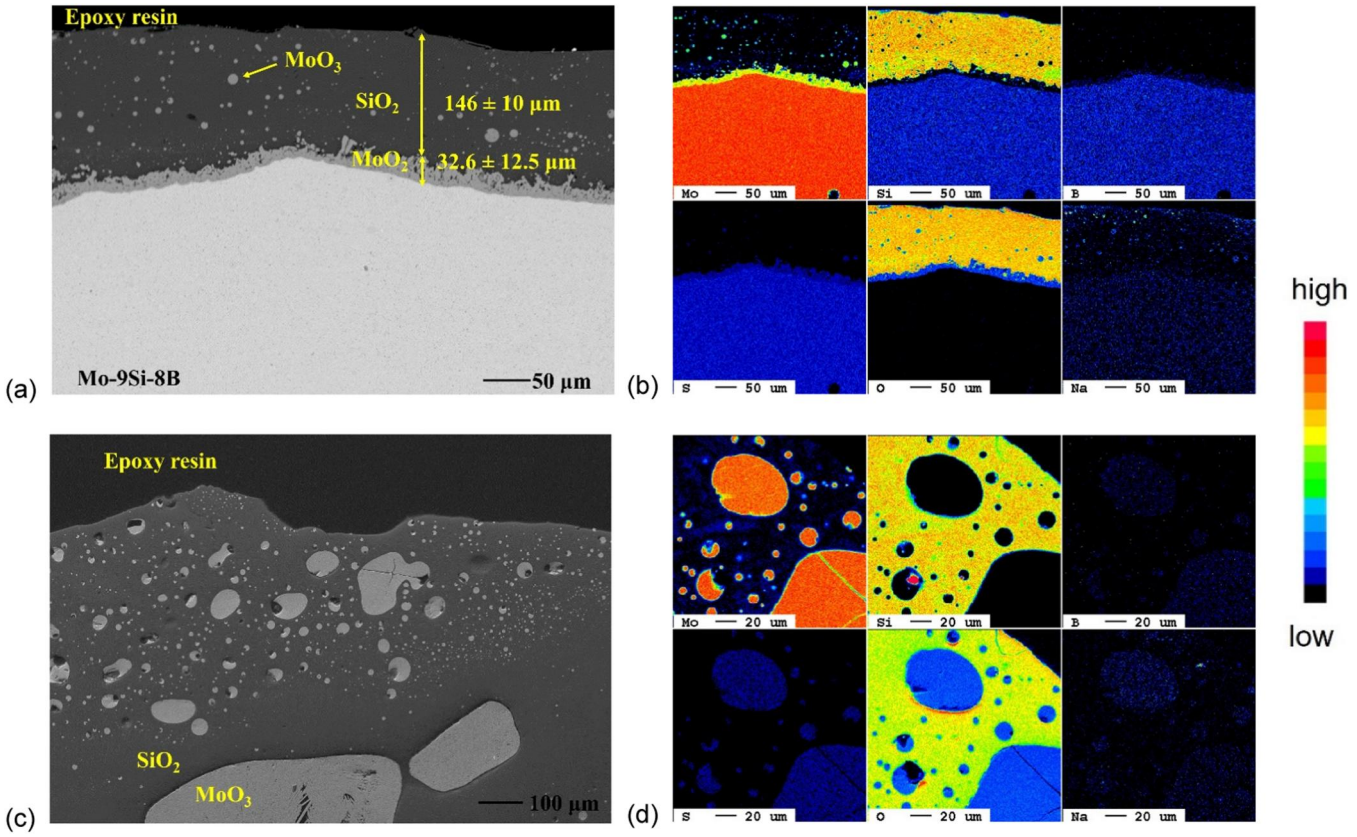

FIGURE 5 | (a, c) BSE images and (b, d) EPMA elemental map of the cross section of Mo-9Si-8B (at.%) after 24 h (a, b) and after 100 h (c, d) of hot corrosion at 900°C with 2.5 mg/cm^2 Na_2SO_4 deposit in synthetic air + 0.1% SO_2. Adapted from [29] - note the varying magnifications. [Color figure can be viewed at wileyonlinelibrary.com]

TABLE 1 | Change in thickness in mm while 24 h and 100 h of hot corrosion of Mo-9Si-8B (at.%) with 2.5 mg/cm^2 Na_2SO_4 deposit in synthetic air + vol. 0.1% SO_2.

Time	500°C	600°C	700°C	800°C	900°C
24 h	0.05 ± 0.01	0.17 ± 0.01	0.30 ± 0.02	1.94 ± 0.04	0.85 ± 0.07
100 h	0.14 ± 0.01	0.32 ± 0.01	0.36 ± 0.01	Consumed	Consumed

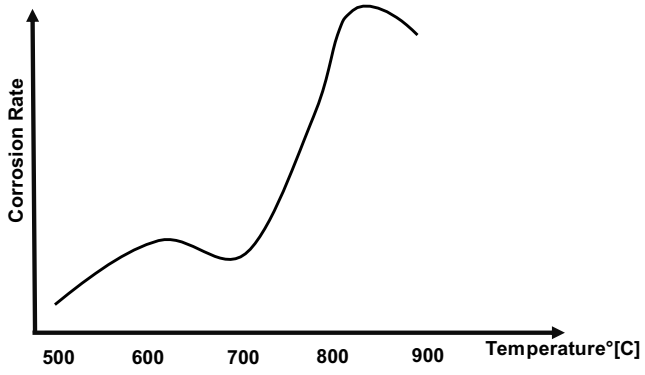

FIGURE 6 | Estimated hot corrosion curve for Mo-9Si-8B (at.%).

5 | Conclusion

The hot corrosion behavior of a Mo-9Si-8B alloy with 2.5 mg/cm^2 Na_2SO_4 deposit in synthetic air + 0.1% SO_2 was investigated between 500°C and 900°C. The main corrosion mechanisms were identified to be influenced by the formation of a eutectic liquid phase, pesting and fluxing, hindering the formation of a protective scale.

Although the formation of the low-melting phase is similar to that of Ni-based alloys, it does not form from sulfate, but from super-acidic molybdates. Sulfur did not interact with the alloy at any temperature. Above 700°C, the corrosion rate also rises with increasing temperature due to pesting, which becomes increasingly dominant up to 900°C. Therefore, the corrosion rate is represented by a temperature-dependent curve different from that known from investigations on the hot corrosion behavior of Ni-based alloys with the typical local maxima of Type I and Type II hot corrosion. Even though a local minimum can be found for this specific alloy, the underlying mechanisms differ from the known Type I and Type II hot corrosion.

To mitigate the corrosion, protection against the formation of the liquid phase needs to be developed. For example, this could involve binding Mo inside another protective oxide, as demonstrated with $Cr_2Mo_3O_{12}$ or $NiMoO_4$. Unfortunately, these compounds are also unstable at temperatures above 810°C [43, 44]. Another method could involve using other oxide formers since the formed oxide does not protect the alloy. These formers are highly acidic oxides themselves, but with better high temperature stability such as tantalates [45].

Author Contributions

Lukas Korell: investigation, writing – original draft preparation, visualization. **Katharina Beck:** methodology, writing – review and editing. **Ceyhun Oskay:** writing – review and editing, supervision. **Daniel Schliephake:** sample preparation. **Martin Heilmaier:** writing – review and editing, project administration, funding acquisition. **Mathias C. Galetz:** conceptualization, writing – review and editing, supervision, project administration, funding acquisition.

Acknowledgements

The authors thank Dr. Gerald Schmidt for EPMA measurements and Mathias Röhrig for technical support. This work was supported by the Research Training Group 2561 "MatCom-ComMat: Materials Compounds from Composite Materials for Applications in Extreme Conditions" (project number: 413956820) funded by the Deutsche Forschungsgemeinschaft (DFG). Open Access funding enabled and organized by Projekt DEAL.

Conflicts of Interest

The authors declare no conflicts of interest.

Data Availability Statement

The data that support the findings of this study are available from the corresponding author upon reasonable request.

References

1. L. Jiang, B. Zheng, C. Wu, et al., "A Review of Mo-Si Intermetallic Compounds as Ultrahigh-Temperature Materials," *Processes* 10 (2022): 1772.

2. J. H. Perepezko, "The Hotter the Engine, the Better," *Science* 326 (2009): 1067–1068.

3. B. Rapp, "Coatings Improve Efficiency," *Materials Today* 9 (2006): 6.

4. D. M. Berczik, "Method for Enhancing the Oxidation Resistance of a Molybdenum Alloy, and a Method of Making a Molybdenum Alloy," *US Patent* 5 (1997): 595–616.

5. M. Akinc, M. K. Meyer, M. J. Kramer, A. J. Thom, J. J. Huebsch, and B. Cook, "Boron-Doped Molybdenum Silicides for Structural Applications," *Materials Science and Engineering: A* 261, no. 1–2 (1999): 16–23.

6. D. M. Dimiduk and J. H. Perepezko, "Mo-Si-B Alloys: Developing a Revolutionary Turbine-Engine Material," *MRS Bulletin* 28, no. 09 (2003): 639–645.

7. D. Schliephake, A. Kauffmann, X. Cong, et al., "Constitution, Oxidation and Creep of Eutectic and Eutectoid Mo-Si-Ti Alloys," *Intermetallics* 104 (2019): 133–142.

8. N. Eliaz, G. Shemesh, and R. M. Latanision, "Hot Corrosion in Gas Turbine Components," *Engineering Failure Analysis* 9 (2002): 31–43.

9. D. A. Shifler, "Hot Corrosion: A Modification of Reactants Causing Degradation," *Materials at High Temperatures* 35 (2018): 225–235.

10. G. H. Meier, "Invited Review Paper in Commemoration of over 50 Years of Oxidation of Metals: Current Aspects of Deposit-Induced Corrosion," *Oxidation of Metals* 98 (2022): 1–41.

11. W. T. Reid, *External Corrosion and Deposits: Boilers and Gas Turbines* (American Elsevier Publishing Co., Inc, 1971).

12. M. Taylor and J. H. Perepezko, "Hot Corrosion of Mo-Si-B Coatings," *Oxidation of Metals* 87 (2017): 705–715.

13. F. Pettit, "Hot Corrosion of Metals and Alloys," *Oxidation of Metals* 76 (2011): 1–21.

14. B. S. Lutz, J. M. Alvarado-Orozco, L. Garcia-Fresnillo, and G. H. Meier, "Na2SO4-Deposit-induced Corrosion of Mo-Containing Alloys," *Oxidation of Metals* 88 (2017): 599–620.

15. B. Grégoire, X. Montero, M. C. Galetz, G. Bonnet, and F. Pedraza, "Mechanisms of Hot Corrosion of Pure Nickel at 700°C: Influence of Testing Conditions," *Corrosion Science* 141 (2018): 211–220.

16. P. Kofstad and G. Akesson, "Sulfate-Induced High-Temperature Corrosion of Nickel," Oxidation of Metals (1980), 14 301–323.

17. R. A. Rapp, "Hot Corrosion of Materials: A Fluxing Mechanism?," *Corrosion Science* 44 (2002): 209–221.

18. H.-H. Strehblow, V. Maurice, and P. Marcus, *Passivity of Metals* (CRC Press, 2011). 3.

19. N. S. Bornstein, "Reviewing Sulfidation Corrosion-Yesterday and Today," *JOM* 48 (1996): 37–39.

20. J. Stringer, "High-Temperature Corrosion of Superalloys," *Materials Science and Technology* 3 (1987): 482–493.

21. S. Obert, A. Kauffmann, and M. Heilmaier, "Characterisation of the Oxidation and Creep Behaviour of Novel Mo-Si-Ti Alloys," *Acta Materialia* 184 (2020): 132–142.

22. S. Obert, A. Kauffmann, R. Pretzler, D. Schliephake, F. Hinrichs, and M. Heilmaier, "The Creep and Oxidation Behaviour of Pesting-Resistant (Mo, Ti)5Si3-containing Eutectic-Eutectoid Mo-Si-Ti Alloys," *Metals* 11 (2021): 169.

23. S. Obert, A. Kauffmann, S. Seils, et al., "Microstructural and Chemical Constitution of the Oxide Scale Formed on a Pesting-Resistant Mo-Si-Ti Alloy," *Corrosion Science* 178 (2021): 109081.

24. F. Hinrichs, A. Kauffmann, A. S. Tirunilai, et al., "A Novel Nitridation-And Pesting-Resistant Cr-Si-Mo Alloy," *Corrosion Science* 207 (2022): 110566.

25. G. C. Fryburg, F. J. Kohl, C. A. Stearns, and W. L. Fielder, "Chemical Reactions Involved in the Initiation of Hot Corrosion of b-1900 and Nasa-Trw via," *Journal of the Electrochemical Society* 129 (1982): 571–585.

26. A. K. Misra, "Mechanism of Na_2SO_4 - Induced Corrosion of Molybdenum Containing Nickel-Base Superalloys at High Temperatures: I, Corrosion in Atmospheres Containing Only," *Journal of the Electrochemical Society* 133 (1986): 1029–1038.

27. K. Beck, T. König, E. Senvardarli, F. Hinrichs, M. Heilmaier, and M. C. Galetz, "Hot Corrosion Behavior of Mo–Si–Ti Alloys," *Materials and Corrosion* 75 (2024): 1610–1619.

28. L. Korell, C. Oskay, G. Falcão, M. Heilmaier, and M. C. Galetz, "Hot Corrosion Behavior of Two Mo-Si-Ti Alloys at Different Temperatures," *Corrosion Science* 271 (2026): 114136.

29. K. Beck, T. König, A. Case, C. Oskay, and M. C. Galetz, "Hot Corrosion Behavior of Mo–9.0Si–8.0B," *Materials and Corrosion* 75 (2024): 1600–1609.

30. T. A. Parthasarathy, M. G. Mendiratta, and D. M. Dimiduk, "Oxidation Mechanisms in Mo-Reinforced Mo5SiB2(T2)–Mo3Si Alloys," *Acta Materialia* 50, no. 2001 (2002): 1857–1868.

31. V. Supatarawanich, D. R. Johnson, and C. T. Liu, "Effects of Microstructure on the Oxidation Behavior of Multiphase Mo–Si–B Alloys," *Materials Science and Engineering: A* 344 (2003): 328–339.

32. C. Hochmuth, D. Schliephake, R. Völkl, M. Heilmaier, and U. Glatzel, "Influence of Zirconium Content on Microstructure and Creep Properties of Mo-9Si–8b Alloys," *Intermetallics* 48 (2014): 3–9.

33. A. Navrotsky and O. J. Kleppa, "Calorimetric Study of Molten Sodium Molybdate-Molybdenum Trioxide Mixtures at 970 °K," *Inorganic Chemistry* 90 (1967): 2119–2121.

34. F. Hoermann, "Beitrag zur Kenntnis der Molybdate und Wolframate. Die Binären Systeme: Li3MoO4-MoO3, Na2MoO4-MoO3, K3MoO4-MoO3, Li2WO4-WO3, Na2WO4-WO3, K2WO4-WO3, Li2MoO4-Na2MoO4, Li2WO4-Na2WO4, Li2moo4-k2moo4," *Zeitschrift für Anorganische und Allgemeine Chemie* 177 (1929): 145–186.

35. K. D. Singh Mudher, M. Keskar, K. Krishnan, and V. Venugopal, "Thermal and X-Ray Diffraction Studies on Na2MoO4, Na2Mo2O7 and Na2Mo4O13," *Journal of Alloys and Compounds* 396 (2005): 275–279.

36. E. Groschuff, "Über Wasserfreie Molybdate I," *Zeitschrift für Anorganische Chemie* 58 (1908): 113–119.

37. R. Amin, Solid State Electrochemical Characterization of Thermodynamic Properties of Sodium-metal-oxygen Systems, Ph.D. thesis, Universität Stuttgart, 2005.

38. Y. K. Voronko, A. A. Sobol, and V. E. Shukshin, "Raman Scattering Study of Molten Alkali-Metal Molybdates Ricn in MoO3," *Inorganic Materials* 50 (2014): 844–849.

39. S. Cole, "The Conversion of Quartz Into Cristobalite below 1000°C, and Some Properties of the Cristobalite Formed," *Journal of the American Ceramic Society* 18 (1935): 149–154.

40. A. Abd el-Moneim, "Quantitative Analysis of Elastic Moduli and Structure of B2O3–SiO2 and Na2O–B2O3–SiO2 Glasses," *Physica B: Condensed Matter* 325 (2003): 319–332.

41. K. Pan, Y. Yang, S. Wei, et al., "Oxidation Behavior of Mo-Si-B Alloys at Medium-to-High Temperatures," *Journal of Materials Science & Technology* 60 (2021): 113–127.

42. M. Hubert and A. Faber, "On the Structural Role of Boron in Borosilicate Glasses," *European Journal of Glass Science and Technology Part B Physics and Chemistry of Glasses* 55 (2014): 136–158.

43. J. Walczak, M. Kurzawa, and E. Filipek, "Studies on Chromium (III) Molybdate and Equilibria in the CrVO4-Cr2 (MoO4) 3 System," *Thermochimica Acta* 150, no. 1 (1989): 133–140.

44. L. Korell, K. Beck, A. R. Chitra, et al., "Type Ii Hot Corrosion of Two Mo-Si-Ti Alloys and Mo-Si-B With a Salt Deposit of Mixed Na2SO4 and NiSO4," *Materials and Corrosion* 77, no. 2 (2026): 177–187.

45. F. Lanoy, E. M. White, B. Schäfer, et al., "Influence of the Cr to Ti Ratio on the High-Temperature Oxidation Behavior of TaMoCrTiAl Complex Concentrated Alloys in Nitrogen-Free Atmospheres," *Materials and Corrosion* 77 (2025): 442–452.

46. T. Sheng, B. Cao, Y. Zhang, and H. Zhang, "New Growth Modes of Molybdenum Oxide Layered 1d Structures Using Alternative Catalysts: Transverse Mode Vs. Axial Mode," *CrystEngComm* 17 (2015): 1139–1150.

Appendix

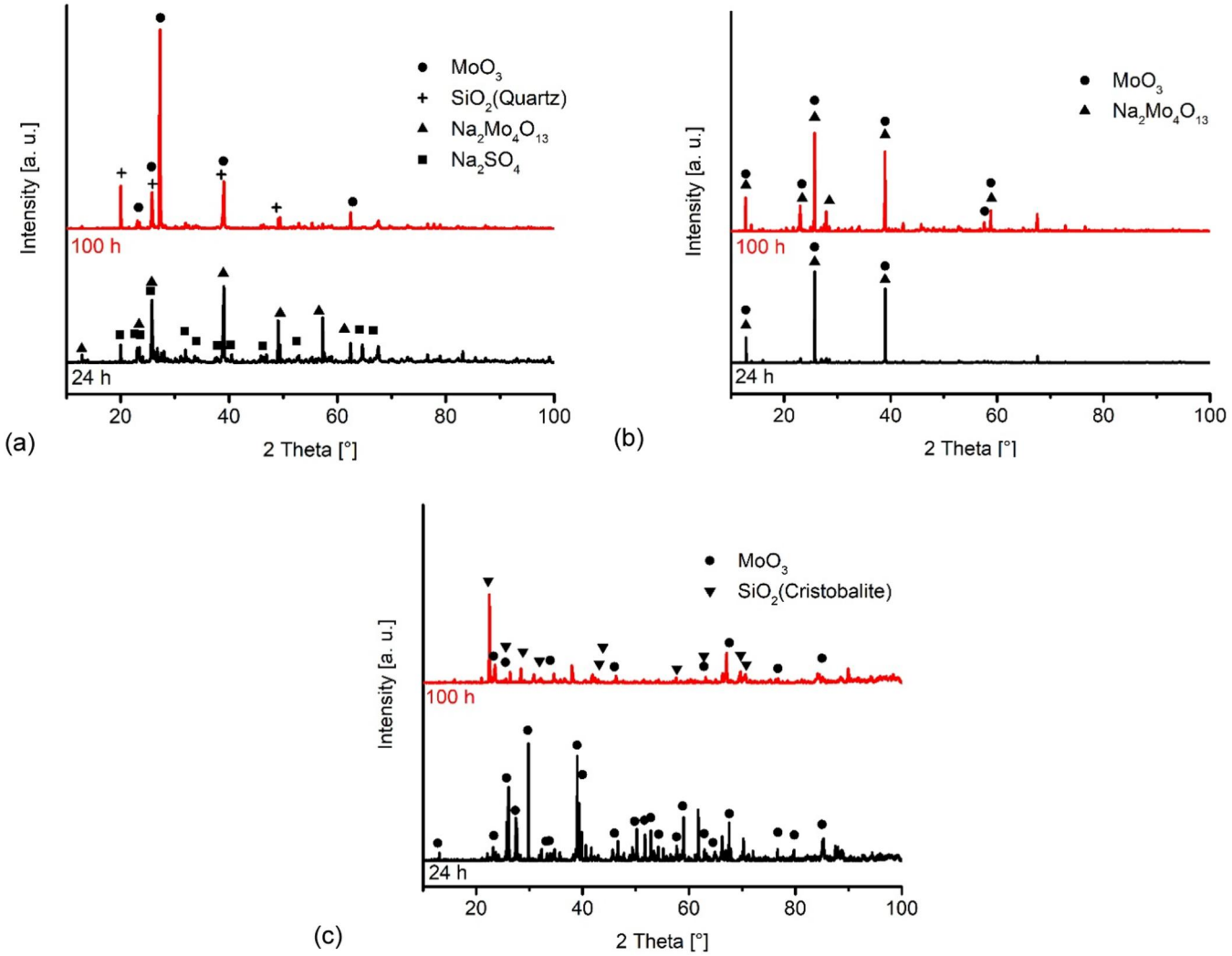

FIGURE A1 | XRD patterns Mo-9Si-8B (at.%) after 24 h and 100 h of hot corrosion test with 2.5 mg/cm^2 Na_2SO_4 deposit in synthetic air + 0.1% SO_2 at (a) 500°C, (b) 600°C and (c) 800°C. [Color figure can be viewed at wileyonlinelibrary.com]

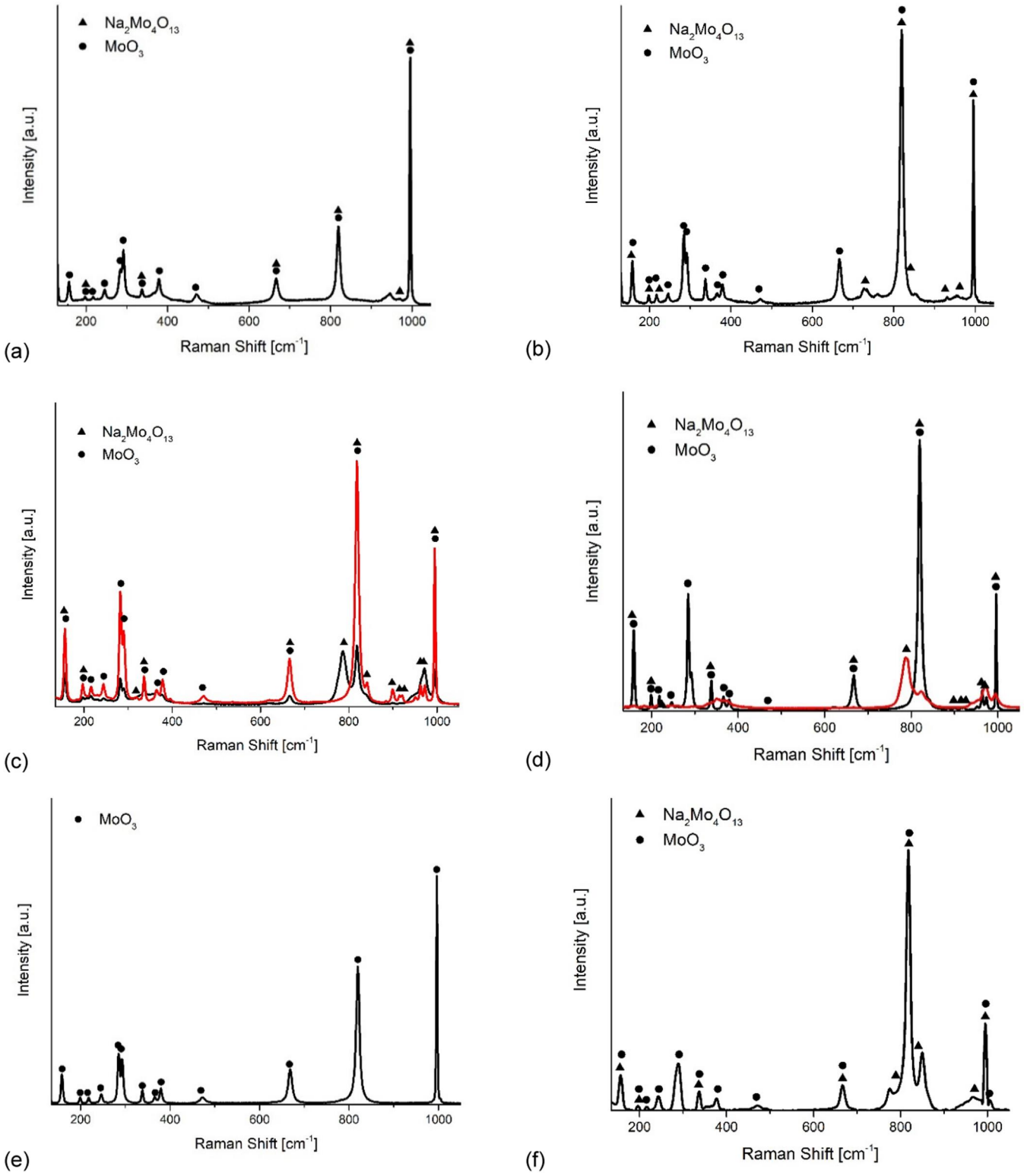

FIGURE A2 | Raman spectroscopy results of Mo-9Si-8B (at.%) after hot corrosion test with 2.5 mg/cm^2 Na_2SO_4 deposit in synthetic air + 0.1% SO_2 for (a) 24 h at 500°C, (b) 100 h at 500°C, (c) 24 h at 600°C, (d) 100 h at 600°C, (e) 24 h at 800°C and (f) 100 h at 800°C. Phases were identified using [46]. [Color figure can be viewed at wileyonlinelibrary.com]